Hindawi
Wireless Communications and Mobile Computing
Volume 2018, Article ID 2525492, 12 pages
https://doi.org/10.1155/2018/2525492

Research Article

Exploiting Impacts of Intercell Interference on SWIPT-Assisted Non-Orthogonal Multiple Access

Thanh-Luan Nguyen[1] **and Dinh-Thuan Do**[2]

[1]*Faculty of Electrical and Electronics Engineering, Bach Khoa University, Ho Chi Minh City, Vietnam*
[2]*Wireless Communications Research Group, Faculty of Electrical and Electronics Engineering, Ton Duc Thang University, Ho Chi Minh City, Vietnam*

Correspondence should be addressed to Dinh-Thuan Do; dodinhthuan@tdt.edu.vn

Received 11 February 2018; Accepted 6 November 2018; Published 25 November 2018

Guest Editor: Shao-Yu Lien

In this paper, we examine the influence of intercell interference (ICI) on the system outage behavior with important derived results in the proposed model of simultaneous wireless information and power transfer (SWIPT) together with the nonorthogonal multiple access (NOMA) using the amplify-and-forward protocol. We derive the closed-form expression of coverage probability for two NOMA users as a function of the signal-to-interference-plus-noise ratio (SINR). To fully take into account the effect of ICI, we adopt more practical parameters to evaluate the optimal power splitting coefficient regarding energy harvesting system performance analysis. Furthermore, to consider a more practical scenario, based on the fact that the number of ICI sources can affect wireless powered relays, we investigate the average outage probability by considering impacts of the reasonable number of participating ICI.

1. Introduction

In recent years, as a significant technique in forthcoming 5G transmission, nonorthogonal multiple access (NOMA) has more attraction due to its opportunity to improve substantial spectrum efficiency (SE) [1]. Considering advantages of power domain allocation to gain simultaneous access for diversified data streams to network, NOMA is evaluated as having better performance than the conventional orthogonal multiple access (OMA) [2]. Concentrating on the SE improvement, many earlier works regarding NOMA scheme are primarily focused. For example, single-input, single-output (SISO) schemes are studied for deployment in cooperative NOMA [3, 4]. In principle, by distributing multiple users into the different power domains, signal intending for the NOMA scheme at the source superimposes the symbol data to serve multiple users at destination. At the receiver, in order to detect multiplexed users' information, successive interference cancellation (SIC) is acquired to eliminate the interference term. In addition to spectrum employment, other metrics need be considered, i.e., user fairness evaluating to multiple users in NOMA. Unlike traditional water-filling power allocation, NOMA users with better channel qualities are allocated less power while more power is allocated to users with poor channel qualities to highlight an enhanced trade-off between model throughput and user fairness. As a result, the same frequency and spreading codes are deployed in a lot of user equipment simultaneously; however they are distinguished by different power levels. Such principle results in improved spectral efficiency and ensured user fairness. The multiple-input-multiple-output (MIMO) NOMA designs are investigated in terms of the ergodic capacity maximization and an optimal power allocation strategy was then proposed as in [5]. The outage performance and the ergodic achievable rate are metrics to consider system performance of cellular downlink NOMA communications. Capacity is another metric to consider performance of NOMA as in [6]. Recently, stochastic geometry networks have been employed in NOMA to exhibit the physical layer security as in [7]. As an extension of [7], single-antenna and multiple-antenna stochastic geometry networks were investigated in two proposed schemes to increase the secrecy performance [8].

In [9], the popular metrics including optimal designs of decoding order, transmission rates, and power allocated to each user are studied in a new design of NOMA under secrecy considerations.

Regarding the idea of combining NOMA with wireless powered networks, NOMA can be deployed with the wireless power transfer; i.e., the simultaneous wireless information and power transfer (SWIPT) technique was presented together with relaying network and its outage performance is considered in [10]. As a promising technology, to prolong the lifetime of energy-constrained users, wireless power transfer is facilitated in wireless relaying networks to forward a signal to far users [11–13]. To permit energy-limited users scavenge energy and information from the transmitted radio frequency (RF) signals, two famous policies, namely, time switching (TS) and power splitting (PS) receiver architecture, are introduced as in [14]. As a scenario of green NOMA, a SWIPT-assisted cooperative NOMA (SWIPT-CNOMA) network is studied as a combination between the NOMA and SWIPT scheme [15], and such novel scheme can be employed to wireless sensor or cellular networks. In such topology, it is possible to avoid lifetime limitation of the energy-constrained NOMA user that acts as a relay which can be able to harvest energy from the received signals. The main benefit of the SWIPT NOMA can be appreciated in the scenario where the relay employs that harvested energy rather than itself to forward the signal to the far NOMA users. In addition, to serve the near NOMA users with strong channel conditions, a PS protocol was employed in the SWIPT-CNOMA system [15]. By revealing the received information in the PS protocol, energy is first harvested and then used to help the signal forwarded to serve the far NOMA users. However, a shortcoming of the PS protocol [15] can be raised in which the relay always retains a quiet slot for some target data rate requirements. Considering the locations of NOMA users, three NOMA user selection policies are performed, including random near NOMA user and random far NOMA user (RNRF) selection, nearest near NOMA user and nearest far NOMA user (NNNF) selection, and nearest near NOMA user and farthest far NOMA user (NNFF) selection. In order to obtain the better outage performance, the authors in [16] considered a best-near best-far NOMA user collection scheme.

However, there are few works that focus on interference effects on the NOMA system. Regarding the influences of cochannel interference (CCI) on the system performance, many outcomes in the literature showed that the aggressive frequency reuse is considered as main reason for CCI in the conventional cellular relaying systems [17–19]. However, FD schemes are more vulnerable to CCI due to the higher frequency reuse, and such characterization exhibits comparison between full-duplex (FD) transmission mode and traditional half-duplex (HD) transmission mode. In addition, in a multicell FD relay base stations meet influences with a much higher CCI due to adjacent cells compared with its HD counterparts [20–22]. As an alternative method, MIMO FD relaying transmission was introduced to examine the harmful effect of CCI on the system performance and such system can be applied in theoretical and practical applications. In [20], to evaluate the average spectral efficiency, a stochastic geometry is conveyed to consider the situation in which the base stations and user equipment operate in small cell network FD mode with FD mode (i.e., the dedicated antennas for transmission and reception are equipped in such FD nodes). In [21, 22], the authors studied the outage probability of a decode-and-forward FD relay with single-antenna nodes in FD relaying subject to CCI. It is worth noting that all these studies are restricted by employing a single antenna in each node of relaying networks. Therefore, deploying multiple receive and transmit antennas at the FD relay is a powerful scheme to eliminate both the CCI and loop interference channels at the FD relay and hence reliability and capacity are achieved.

However, to the best of our knowledge, the impact of ICI on the performance of CNOMA with capability of energy harvesting has yet to be fully pressed. Such analysis motivates us to find impacts of ICI on the SWIPT-assisted NOMA.

The primary contributions of our paper are summarized as follows:

(i) Different from the system model presented in [10, 14] where the relay only harvests energy from one source (i.e., base station), by deploying ICI as an extra resource to feed energy for relay, we propose a new SWIPT NOMA protocol under impacts of ICI to enhance the level of harvested energy to prolong the lifetime of NOMA systems

(ii) We derive closed-form expressions for the outage probability at NOMA users, when considering the interference channel schemes

(iii) The optimal power splitting factor is derived to obtain the maximum coverage probability at each user in SWIPT NOMA

The rest of the paper is structured as follows. In Section 2, the system model for studying cooperative SWIPT NOMA is introduced. In Section 3, new analytical expressions are derived for the outage probability when the proposed scheme is used. The optimal power splitting factor for SWIPT can be shown in Section 4. Numerical results are offered in Section 5, which is followed by the conclusion in Section 6.

2. System Model

Consider a SWIPT NOMA network with the help of an energy-constrained relay for transmission to two representative NOMA users considering impacts of external interferers to the relay. In particular, Figure 1 illustrates the proposed system model, where one source node (s), i.e., the main base station, one EH-assisted relay (r), and two users are considered. The relay utilizes the amplify-and-forward (AF) relaying protocol to transmit the superimposed signals from the source to each user and the power splitting (PS) protocol is adopted for energy harvesting. The channel between node x and node y is assumed to experience Rayleigh fading where $\Omega_{xy} = \mathbb{E}[|h_{xy}|^2]$ is the average channel

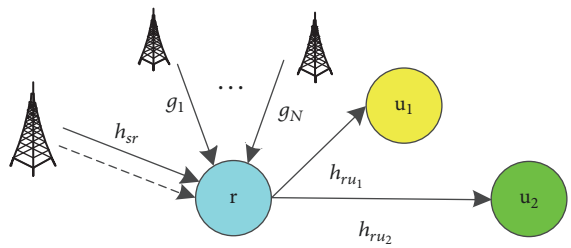

FIGURE 1: System model.

power gain. Each node is equipped with a single half-duplex antenna.

Assume that the relay is affected by N external interferers. The channel coefficient between the n-th interferer and the relay is modeled as Nakagami-m fading with shape factor m_n and variance of $\Omega_n = \mathbb{E}[|g_n|^2]$, i.e., $g_n \sim \Gamma(m_n, \Omega_n/m_n)$. All given channels are assumed to be independent and not necessarily identically distributed. The transmission between the source and two users is divided into two phases. In the first phase, the source broadcasts a superimposed mixture of signals, i.e., $x_s = \sqrt{\alpha_1}x_1 + \sqrt{\alpha_2}x_2$, where x_i, $i \in \{1,2\}$, is the intended signal for user u_i, $\alpha_1 + \alpha_2 = 1$.

Assuming that the relay utilizes the power splitting (PS) protocol for energy harvesting [11], thus the received signal at the relay node is given by

$$y_r = \sqrt{(1-\beta)P_s}x_s h_{sr} + \sum_{n=1}^{N}\sqrt{(1-\beta)P_n}g_n x_n + n_r, \quad (1)$$

where $\beta \in (0,1)$ is the power splitting ratio, P_s is the transmit power of the source, x_n and P_n are signal and the transmit power of the n^{th} interferer, respectively, and n_r is the zero mean additive white Gaussian noise (AWGN) at the relay with variance of σ^2. Specifically, the harvested energy at the relay node is obtained as

$$E_h = \eta\beta\left(P_s|h_{sr}|^2 + \sum_{n=1}^{N}P_n|g_n|^2\right)\frac{T}{2}, \quad (2)$$

where $\eta \in [0,1]$ is a coefficient representing the efficiency of the harvesting circuitry and T is the block time for the transmission from the source node to both users. Therefore, the transmit power at the relay is obtained as

$$P_r = \frac{E_h}{T/2} = \eta\beta\left(P_s|h_{sr}|^2 + \sum_{n=1}^{N}P_n|g_n|^2\right). \quad (3)$$

In the second phase, the relay multiplies the received signal with an amplifying gain G and then forwards the amplified signal to both users. Hence, the received signal at user$i$ is given by

$$\begin{aligned} y_i &= \sqrt{P_r}y_r h_{ru_i}G + n_i \\ &= \sqrt{P_r}h_{ru_i}\left(\sqrt{(1-\beta)P_s}x_s h_{sr}\right)G \\ &\quad + \sqrt{P_r}h_{ru_i}\left(\sum_{n=1}^{N}\sqrt{(1-\beta)P_n}g_n x_n\right)G \\ &\quad + \sqrt{P_r}h_{ru_i}n_r G + n_i, \end{aligned} \quad (4)$$

where n_i is the zero mean additive white Gaussian noise (AWGN) at user u_i with variance of σ^2. The amplifying factor due to the AF protocol at the relay is given by

$$G = \frac{1}{\sqrt{(1-\beta)P_s|h_{sr}|^2 + (1-\beta)\sum_{n=1}^{N}P_n|g_n|^2 + \sigma^2}}. \quad (5)$$

Remark 1. Without loss of generality, we assume that user u_1 has better channel quality than user u_2; i.e., $|h_{ru_2}|^2 \le |h_{ru_1}|^2$. Hence, due to NOMA, user 1 is encouraged to priorly decode x_2 before detecting its own signal by applying successive interference cancellation (SIC), while user 2 can directly detect x_2.

Due to Remark 1, the instantaneous signal-to-interference-plus-noise ratio (SINR) at user 1 to detect user 2's signal is given by

$$\gamma_{1\to 2} = \frac{\alpha_2 P_s|h_{sr}|^2}{\alpha_1 P_s|h_{sr}|^2 + \sum_{n=1}^{N}P_n|g_n|^2 + \left(\sigma^2/P_r G^2\right)/(1-\beta)\left|h_{ru_1}\right|^2 + \sigma^2/(1-\beta)}. \quad (6)$$

Lemma 2. *The term $\sigma^2/P_r G^2$ can be approximated in the high signal-to-noise ratio (SNR) region, in which the source transmits with a relatively large power, as*

$$\frac{\sigma^2}{P_r G^2} \simeq \frac{(1-\beta)\sigma^2}{\eta\beta}. \quad (7)$$

Proof. By substituting (3) and (5) into $\sigma^2/P_r G^2$ we have

$$\begin{aligned} \frac{\sigma^2}{P_r G^2} &= \frac{\left((1-\beta)P_s|h_{sr}|^2 + (1-\beta)\sum_{n=1}^{N}P_n|g_n|^2\right)\sigma^2}{\eta\beta\left(\mathscr{P}_s|h_{sr}|^2 + \sum_{n=1}^{N}P_n|g_n|^2\right)} \\ &\quad + \frac{\sigma^4}{\eta\beta\left(P_s|h_{sr}|^2 + \sum_{n=1}^{N}P_n|g_n|^2\right)}. \end{aligned} \quad (8)$$

Note that, in the high SNR region, the second term, i.e., $\sigma^4/\eta\beta(P_s|h_{sr}|^2 + \sum_{n=1}^{N} P_n|g_n|^2)$, can be neglected. Hence, after ignoring this part, we can simply achieve the result of Lemma 2.

Therefore, the approximated instantaneous $\gamma_{1\longrightarrow 2}$ is obtained by

$$\gamma_{1\longrightarrow 2} \approx \frac{\alpha_2\psi_{sr}}{\alpha_1\psi_{sr} + \psi_I + 1/\psi_{ru_1} + 1/(1-\beta)}, \tag{9}$$

where $\psi_{sr} \triangleq P_s|h_{sr}|^2/\sigma^2$, $\psi_I \triangleq \sum_{n=1}^{N} P_n|g_n|^2/\sigma^2$, and $\psi_{ru_1} \triangleq \eta\beta|h_{ru_1}|^2$. If $\gamma_{1\longrightarrow 2} > 2^{2R_2} - 1$, where R_2 (bits/s/Hz) is the target data rate for u_2, user 1 can successfully carry out the successive interference cancellation (SIC) technique to detect user 2's signal and remove this signal from y_1. Assuming perfect SIC, the approximated instantaneous SINR for user 1 to detect its own signal is given by

$$\gamma_1 \approx \frac{\alpha_1\psi_{sr}}{\psi_I + 1/\psi_{ru_1} + 1/(1-\beta)}. \tag{10}$$

Note that if $\gamma_1 > 2^{2R_1} - 1$, where R_1 (bits/s/Hz) is the target data rate for u_1, user 1 can successfully decode its own message. Similarly, the SINR at user 2 to detect its signal is obtained as

$$\gamma_2 = \frac{\alpha_2 P_s |h_{sr}|^2}{\alpha_1 P_s |h_{sr}|^2 + \sum_{n=1}^{N} P_n |g_n|^2 + (\sigma^2/P_r G^2)/(1-\beta)\,|h_{ru_2}|^2 + \sigma^2/(1-\beta)}. \tag{11}$$

Define $\psi_{ru_2} \triangleq \eta\beta|h_{ru_2}|^2$; the approximated γ_2 achieved by adopting Lemma 2 is given by

$$\gamma_2 \approx \frac{\alpha_2\psi_{sr}}{\alpha_1\psi_{sr} + \psi_I + 1/\psi_{ru_2} + 1/(1-\beta)}. \tag{12}$$

□

3. Performance Analysis

3.1. Preliminaries. In this section, some preliminary results are presented in terms of the solutions of some PDF and/or CDF calculation, which will be frequently invoked in the analysis. Let $Y = \sum_{n=1}^{N} X_n$ be the sum of N independent and not necessarily identically distributed gamma random variables (RVs), i.e., $X_n \sim \Gamma(m_n, \Omega_n/m_n)$, where $\Omega_n = \mathbb{E}[X_n]$.

Theorem 3. *The approximated probability density function (PDF) of Y follows the gamma distribution, where m_I is the shape factor and Ω_I is the variance, which is given by [23–25]*

$$f_Y^{[1]}(\gamma) \approx \frac{1}{\Gamma(m_I)\,\mu_I^{m_I}}\gamma^{m_I-1}\exp\left(-\frac{\gamma}{\mu_I}\right), \quad \gamma \geq 0, \tag{13}$$

where $\mu_I = \Omega_I/m_I$, $\Omega_I = \sum_{n=1}^{N}\Omega_n$. The shape parameter, m_I, is computed by using moment-base estimators, which is given by

$$m_I = \frac{\Omega_I^2}{\mathbb{E}[\Phi^2] - \Omega_I^2}, \tag{14}$$

where the first term in the denominator, $\mathbb{E}[\Phi^2]$, can be obtained with the help of

$$\mathbb{E}\left[\Phi^{k_0}\right] = \sum_{\{k_n\}_{n=1}^{N-1}}^{k_0} \mathbb{E}\left[|X_N|^{2k_{N-1}}\right] \cdot \prod_{t=1}^{N}\binom{k_{t-1}}{k_t}\mathbb{E}\left[|X_{N-1}|^{2(k_{t-1}-k_t)}\right], \tag{15}$$

in which

$$\mathbb{E}\left[|X_n|^k\right] = \frac{\Gamma(m_n + k/2)}{\Gamma(m_n)}\left(\frac{\Omega_n}{m_n}\right)^{k/2}, \tag{16}$$

where $\sum_{\{k_n\}_{n=1}^{N-1}}^{k_0}$ is a short-hand representation of $\sum_{k_1=0}^{k_0}\sum_{k_2=0}^{k_1}\cdots\sum_{k_{N-1}=0}^{k_{N-1}}\cdots$ and $\binom{n}{k}$ denotes the binomial coefficient. In addition, when m_n is a nonnegative integer, the exact PDF and CDF of Y are obtained through Theorem 4 as below.

Theorem 4. *Without loss of generality, we assume that $\mu_1 \geq \mu_2 \geq \ldots \geq \mu_N$, where $\mu_n = \Omega_n/m_n (n = 1 \ldots N)$. Therefore, the exact probability density function (PDF) of Y, where $m_n \in \mathbb{Z}^+$, is given by*

$$f_Y^{[2]}(\gamma) = \sum_{p=1}^{P}\sum_{q=1}^{m_{\langle p\rangle}} \frac{R_{p,q}(\mathcal{S})}{(q-1)!\mu_{\langle p\rangle}^q}\gamma^{q-1}\exp\left(-\frac{\gamma}{\mu_{\langle p\rangle}}\right), \quad \gamma \geq 0, \tag{17}$$

in which $\mathcal{S} = \{\mu_n\}_{n=1}^{N}$ is a vector containing all μ_n's. Without loss of generality, assume that vector $\mathcal{S}$ contains P distinct elements; each element is denoted by $\mu_{\langle p\rangle}$, where $p = 1, 2, \ldots, P$. Intuitively, $m_{\langle p\rangle}$ is the sum of all m_n's ($n \geq 1$), in which the subscript is the index of the n-th element of $\mathcal{S}$, i.e., μ_n, that is identical to $\mu_{\langle p\rangle}$. Specifically, the value of $m_{\langle p\rangle}$ is determined through Figure 2 and the below description.

In Figure 2, τ_p is the number of elements identical to $\mu_{\langle p\rangle}$ and $s_p \triangleq \sum_{k=1}^{p}\tau_k$ and $s_{p-1} + 1$ denote the indices of the last

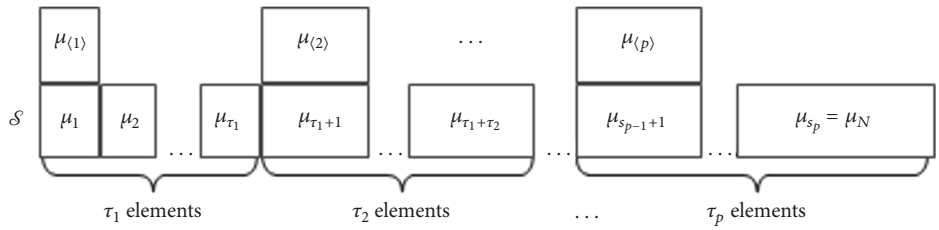

Figure 2: A realization between $\mu_{\langle p\rangle}$ and the elements in vector $\mathcal{S}$.

and the first element identical to $\mu_{\langle p\rangle}$, respectively. Therefore, $m_{\langle p\rangle} = \sum_{k=s_{p-1}+1}^{s_p} m_k$. Subsequently, $R_{p,q}(\mathcal{S})$ is obtained by

$$R_{p,q}(\mathcal{S}) = \frac{1}{\left(m_{\langle p\rangle}-q\right)!\mu_{\langle p\rangle}^{m_{\langle p\rangle}-q}} \times \left(\frac{d^{m_{\langle p\rangle}-q}}{dv^{m_{\langle p\rangle}-q}} \prod_{k=1,k\neq p}^{P} \frac{1}{\left(1+\mu_{\langle k\rangle}v\right)^{m_{\langle k\rangle}}}\right)\Bigg|_{v=-1/\mu_{\langle p\rangle}}. \tag{18}$$

Proof. See Appendix A. □

The closed-form expression of (18) is given in Appendix B in order to find the values of $R_{p,q}(\mathcal{S})$ without requiring any differentiation manipulation. In addition, Remark 5 is given in order to provide some insights of Theorem 4.

Remark 5. Theorem 4 is priorly defined for $m_n \in \mathbb{Z}^+$; however in case of $m_n \in \mathbb{R}^+$ one can still utilize Theorem 4 to find the sum of N i.n.i.d. gamma RVs as long as it satisfies $m_{\langle p\rangle} \in \mathbb{Z}^+$. This statement can be understood by observing the agreement between the simulation curves and analytical curves in Section 5. Further, it is noticed from Appendix A that (A.3) can also extend to the case of $m_n \in \mathbb{R}^+$ without any modification. However, in order to adopt partial fraction decomposition (PFD) to achieve the closed-form expression for $f_Y^{[2]}(\gamma)$ in the third equality of (A.4), $m_{\langle p\rangle} \in \mathbb{Z}^+$ must be a positive integer, which can be easily achieved by assuming $m_n \in \mathbb{Z}^+$ is also a positive integer.

Furthermore, in order to support the analysis in Section 3.2 we introduce Theorem 6 as below.

Theorem 6. *Let* $\mathrm{I}_Y(\kappa) \triangleq \mathbb{E}_Y[e^{-\kappa Y}]$*; its closed-form expression is obtained as*

$$\mathrm{I}_{\psi_I}(\kappa) = \int_0^\infty \mathrm{e}^{-\kappa\gamma} f_Y^{[t]}(\gamma)\, d\gamma \tag{19}$$

$$= \begin{cases} \left(1+\mu_I\kappa\right)^{-m_I} & (t=1) \\ \sum_{p=1}^{P}\sum_{q=1}^{m_{\langle p\rangle}} \dfrac{R_{p,q}(\mathcal{S})}{\left(1+\mu_{\langle p\rangle}\kappa\right)^q} & (t=2). \end{cases} \tag{20}$$

Proof. Using the given PDF of ψ_I in (13) for $t = 1$ and (17) for $t = 2$, with the help of [26, Eq. 3.351.3], we can easily achieve the above results.

In addition, when the interferences are statistically independent and identically distributed (i.i.d.), i.e., $\mu_1 = \mu_2 = \ldots = \mu_N = \mu$, then $P = 1$ and $m_{\langle p\rangle} = \sum_{n=1}^{N} m_n \triangleq m$; $\mathrm{I}_Y(\kappa)$ becomes

$$\mathrm{I}_{\psi_I}(\kappa) = \left(1+\mu\kappa\right)^{-m}. \tag{21}$$

When $N = 0$, i.e., $Y = 0$, it immediately follows that $\mathrm{I}_{\psi_I}(\kappa) = 1$. □

3.2. Performance Analysis on Outage Probability at Each User. In this section, the analytical result for the coverage probability of user u_i, denoted by $\overline{\mathcal{O}}_i$, is given in closed form. Hence, the outage probability at user u_i is $\mathcal{O}_i = 1 - \overline{\mathcal{O}}_i$. It is worth noticing that the results in this section are obtained when $\alpha_2 > \tau_2\alpha_1$ and if $\alpha_2 < \tau_2\alpha_1$ the coverage probability of each user becomes zero. Subsequently, the coverage probability of user 1 is defined as the probability that this user successfully decodes both x_2 and x_1 which is mathematically given by

$$\overline{\mathcal{O}}_1 = \Pr\left\{\gamma_{1\longrightarrow 2} > \tau_2, \gamma_1 > \tau_1\right\}, \tag{22}$$

where $\tau_2 \triangleq 2^{2R_2} - 1$ and $\tau_1 \triangleq 2^{2R_1} - 1$. However, deriving the exact $\overline{\mathcal{O}}_1$ in closed form is not tractable due to the complexity of (6); thus we then derive the approximated coverage probability in the high SNR region by substituting (9) and (10) into (22). Note that this assumption is widely used in literature. Subsequently, this probability is approximately obtained in closed form as

$$\overline{\mathcal{O}}_1 \simeq \mathrm{I}_{\psi_I}\left(\frac{\mathrm{T}_1}{\mu_{sr}}\right)\exp\left(-\frac{\mathrm{T}_1}{\mu_{sr}}\frac{1}{1-\beta}\right) \times \sum_{k=1}^{3}(-1)^{k-1}\, 2\sqrt{\frac{\mathrm{T}_1}{\mu_{sr}\mu_k}}K_1\left(2\sqrt{\frac{\mathrm{T}_1}{\mu_{sr}\mu_k}}\right), \tag{23}$$

where $\mu_{sr} = P_s\Omega_{sr}/\sigma^2$, $\mu_{ru_1} = \eta\beta\Omega_{ru_1}$, $\mu_{ru_2} = \eta\beta\Omega_{ru_2}$, $\mathrm{T}_1 = \max(\tau_2/(\alpha_2 - \tau_2\alpha_1), \tau_1/\alpha_1)$, $\mu_1 = \mu_{ru_1}$, $\mu_2 = \mu_{ru_1}\mu_{ru_2}/\mu_{ru_2} + \mu_{ru_1}$, and $\mu_3 = \mu_{ru_2}$, $\mathrm{I}_{\psi_I}(\kappa)$ is obtained in Theorem 6 and Theorem 4 by setting $\Omega_I = \sum_{n=1}^{N} P_n\Omega_n/\sigma^2$ for $(t = 1)$ and $m_I = \sum_{n=1}^{N} P_n\Omega_n/\sigma^2$, $K_\nu(z)$ is the ν^{th} order modified Bessel function of the second kind [26], and $\alpha_2 > \tau_2\alpha_1$.

Proof. See Appendix C. □

Hence, the coverage probability of user 2 is defined as the probability that this user successfully decodes its own message, x_2, and can be represented mathematically by

$$\overline{\mathcal{O}}_2 = \Pr\left\{\gamma_2 > \tau_2\right\}. \tag{24}$$

Subsequently, the closed-form expression for the approximated $\overline{\mathcal{O}}_2$ is given by

$$\begin{aligned}\overline{\mathcal{O}}_2 \simeq{}& \mathrm{I}_{\psi_I}\left(\frac{\mathrm{T}_2}{\mu_{sr}}\right)\exp\left(-\frac{\mathrm{T}_2}{\mu_{sr}}\frac{1}{1-\beta}\right)\\ &\cdot 2\sqrt{\frac{\mathrm{T}_2}{\mu_{sr}\mu_2}}K_1\left(2\sqrt{\frac{\mathrm{T}_2}{\mu_{sr}\mu_2}}\right),\end{aligned} \tag{25}$$

where $\mathrm{T}_2 = \tau_2/\alpha_2 - \tau_2\alpha_1$ and $\alpha_2 > \tau_2\alpha_1$.

Proof. Substituting (12) into (22), we then obtain

$$\begin{aligned}\overline{\mathcal{O}}_2 &\simeq \Pr\left\{\psi_{sr} > \mathrm{T}_2\left(\psi_I + \frac{1}{\psi_{ru_2}} + \frac{1}{1-\beta}\right)\right\}\\ &\simeq \exp\left(-\frac{\mathrm{T}_2}{\mu_{sr}}\frac{1}{1-\beta}\right)\int_0^\infty \exp\left(-\frac{\mathrm{T}_2}{\mu_{sr}}x\right) f_{\psi_I}^{[t]}(x)\,dx\\ &\quad\times\int_0^\infty \exp\left(-\frac{\mathrm{T}_2}{\mu_{sr}}\frac{1}{y}\right) f_{\psi_{ru_2}}(y)\,dy.\end{aligned} \tag{26}$$

In addition, the first integral is obtained by adopting (20) when $\kappa = \mathrm{T}_2/\mu_{sr}$. Recall that $|h_{ru_2}|^2 \le |h_{ru_1}|^2$ due to Remark 1; thus $\psi_{ru_2} \le \psi_{ru_1}$. Using order statistic in [27], the PDF of the ordered ψ_{ru_2} is given by

$$f_{\psi_{ru_2}}(y) = \frac{1}{\mu_2}\exp\left(-\frac{y}{\mu_2}\right), \quad (y \ge 0). \tag{27}$$

Therefore, the closed-form expression for the second integral is obtained by using (27) and [26, Eq. 3.471.9]. Hence, the proof is done. □

4. Optimal Power Splitting Factor Problem

In this section, the maximum coverage probability at a single user is obtained by adjusting the power splitting factor to maximize the SNRs/SINRs given in Section 3. Specifically, the optimal power splitting factor to achieve the maximum SNRs/SINRs at user u_i is given by

$$\beta_i^{\mathrm{op}} = \arg\max_{0<\beta<1}\left(\varphi_i\right), \tag{28}$$

where $\varphi_1 \triangleq \min\{\gamma_{1\longrightarrow 2}, \gamma_1\}$ and $\varphi_2 \triangleq \gamma_2$. Since β only appears in the denominator of φ_i we can rewrite (28) as

$$\beta_i^{\mathrm{op}} = \arg\min_{0<\beta<1}\left(\psi_i(\beta) \triangleq \frac{1}{\eta\beta\left|h_{ru_i}\right|^2} + \frac{1}{1-\beta}\right). \tag{29}$$

Lemma 7. *The function $\psi_i(\beta)$ is convex.*

Proof. Since $1/\eta\beta|h_{ru_i}|^2$ and $1/1-\beta$ are convex functions of $\beta \in (0,1)$ and the sum of two convex functions is also convex, thus $\psi_i(\beta)$ is convex.

From Lemma 7, it is clear that (30) has a unique solution for β_i^{op} which is obtained by solving $(\partial/\partial\beta)\psi_i(\beta) = 0$. Subsequently, after some simple algebraic manipulations, the optimal energy harvesting factor is given as below:

$$\beta_i^{\mathrm{op}} = \frac{1}{1+\sqrt{\eta\left|h_{ru_i}\right|^2}}. \tag{30}$$

Substituting (30) into (9), (10), and (12), the optimal coverage probability of user u_i is given approximately as

$$\begin{aligned}\overline{\mathcal{O}}_i^{op} \simeq{}& \mathrm{I}_{\psi_I}\left(\frac{\mathrm{T}_i}{\mu_{sr}}\right)\exp\left(-\frac{\mathrm{T}_i}{\mu_{sr}}\right)\sum_{k=i}^{4-i}(-1)^{k+\bar{i}-1}\\ &\cdot\left\{\times\omega_{i,k}K_1\left(\omega_{i,k}\right) - \sqrt{\pi\frac{\mathrm{T}_i}{\mu_{sr}\eta}}\omega_{i,k}\exp\left(-\omega_{i,k}\right)\right\},\end{aligned} \tag{31}$$

where $\omega_{i,k} = 2\sqrt{\mathrm{T}_i/\mu_{sr}\eta\Omega_k}$, $\Omega_1 = \Omega_{ru_1}$, $\Omega_2 = \Omega_{ru_1}\Omega_{ru_2}/\Omega_{ru_1} + \Omega_{ru_2}$, $\Omega_3 = \Omega_{ru_2}$, and $\bar{i} = 2/i$. □

Proof. See Appendix D. □

Note that the relay can only choose to tune β to achieve the best performance for a single user in a specific block time, T; thus the other user may not reach maximum coverage probability during that block time. In this case, the coverage probability of the other user is given approximately by

$$\begin{aligned}\overline{\mathcal{O}}_{\bar{i}} \simeq{}& \mathrm{I}_{\psi_I}\left(\frac{\mathrm{T}_{\bar{i}}}{\mu_{sr}}\right)\exp\left(-\frac{\mathrm{T}_{\bar{i}}}{\mu_{sr}}\right)\\ &\cdot\sum_{k_{\bar{i}}=\bar{i}}^{4-\bar{i}}\sum_{k_i=i}^{4-i}(-1)^{k_{\bar{i}}+i-1}(-1)^{k_i+\bar{i}-1}\\ &\times\left[\left(1-\frac{\mathrm{T}_{\bar{i}}}{\mu_{sr}}\sqrt{\frac{\pi}{\eta\Omega_{k_i}}}\right)\omega_{\bar{i},k_{\bar{i}}}K_1\left(\omega_{\bar{i},k_{\bar{i}}}\right)\right.\\ &\left.-\frac{\mathrm{T}_{\bar{i}}}{\mu_{sr}\Omega_{k_{\bar{i}}}}\sqrt{\frac{\pi\Omega_{k_i}}{\eta}}K_0\left(\omega_{\bar{i},k_{\bar{i}}}\right)\right],\end{aligned} \tag{32}$$

where $\omega_{\bar{i},k_{\bar{i}}} = 2\sqrt{\mathrm{T}_{\bar{i}}/\mu_{sr}\eta\Omega_{k_{\bar{i}}}}$.

Proof. See Appendix E. □

5. Numerical Results

In this section, in terms of the outage probability of both users in the cooperative SWIPT NOMA network, we present representative numerical results to demonstrate the performance assessments. In the considered SWIPT NOMA network under impacts of ICI, we set the energy conversion efficiency of SWIPT as $\eta = 1$. We define SNR $\triangleq P_s\Omega_{sr}/\sigma^2$

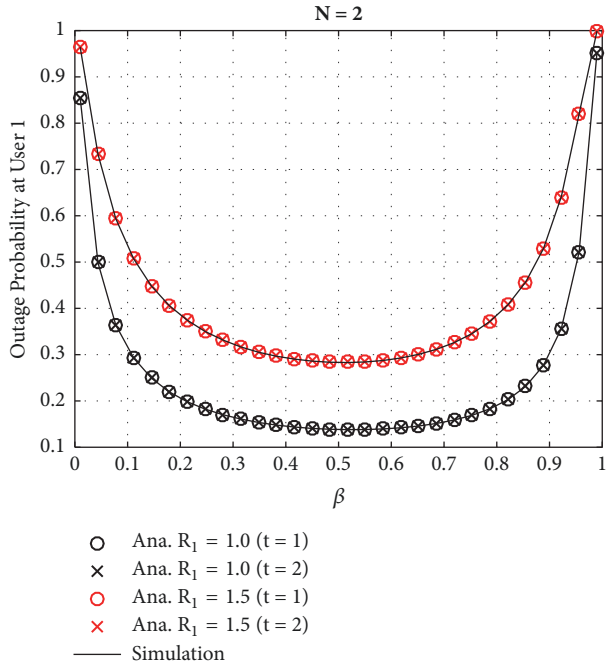

Figure 3: Outage probability at user 1 vs. the energy harvesting ratio β, where SNR = 30 dB and INR = −10 dB.

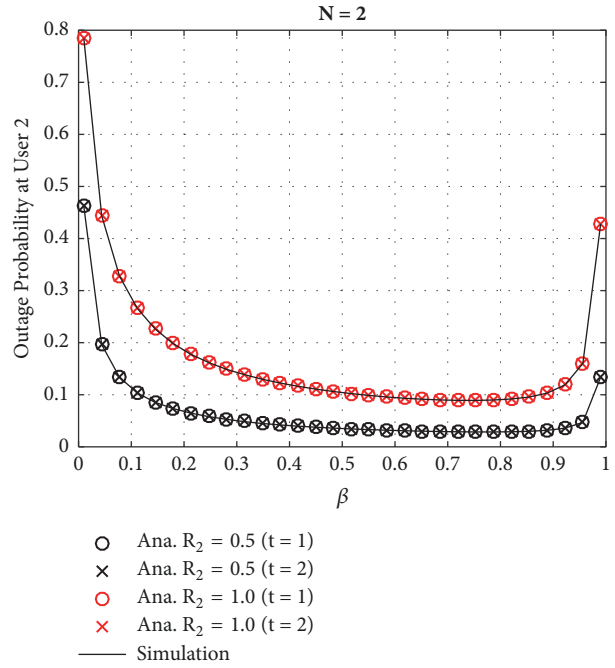

Figure 4: Outage probability at user 2 vs. the energy harvesting ratio β, where SNR = 30 dB and INR = −10 dB.

as the average SNR at the transmitter (source); assume that $P_n = P_I$ and define INR $\triangleq \sum_{n=1}^{N} P_I \Omega_n / \sigma^2$ as the average interference-to-noise ratio. $\Omega_{sr} = 1$, $\Omega_{ru_1} = 1.5$, and $\Omega_{ru_2} = 0.5$. From Figures 3–8, the number of external interferers is set to 2 ($N = 2$) with $m_1 = 1.2$, $m_2 = 1.8$, $\Omega_1 = 1.2$, and $\Omega_2 = 1.8$; the power allocation coefficients are $\alpha_1 = 0.1$ and $\alpha_2 = 0.9$. The below results are obtained by averaging 500,000 separated simulations under a MATLAB environment.

Firstly, we consider the results in Figures 3 and 4. The curves denoted by (O) can be obtained from (23) with $I_{\psi_I}(\kappa)$ in (20) achieved at $t = 1$ whereas the curves denoted by (X) can be obtained with $I_{\psi_I}(\kappa)$ obtained at $t = 2$ (20). As a clear observation, the simulation lines obtained via (22) and (24), respectively, strictly match with the analytical lines for both $t = 1$ and $t = 2$, which confirms the accuracy of our derivation. Furthermore, Figure 3 shows the outage probability for user 1, as increasing R_1 to serve this user with higher data rate or higher quality of service and outage performance will be the worse case. In such result, the black curve is $R_1 = 1.0$ bits/s/Hz while the red curve is $R_1 = 1.5$ bits/s/Hz. One can observe that a lower outage probability is achieved by changing approximate $\beta = 0.6 \longrightarrow 0.8$. The figures also demonstrate that as β is very high or very low, a higher outage event can occur due to the low harvested energy at the relay where it makes impacts on the end-to-end SNR of the system. Similarly, outage probability (not optimal) is shown for user 2 in Figure 4. It can be observed that as R_2 is increased then outage performance will be worse; in this case, we set $R_2 = 0.5$ bits/s/Hz as the black curves and the red ones corresponding with $R_2 = 1.0$ bits/s/Hz.

In Figure 5, the outage probabilities for user 1 are achieved by varying INR levels and are shown as functions of the

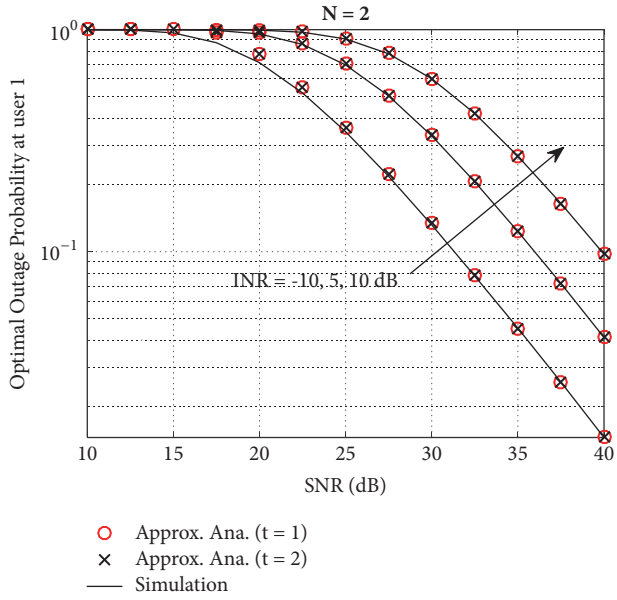

Figure 5: Optimal outage probability at user 1 vs. the average SNR.

average SNR. The simulation curves are obtained by adopting (22) with β defined in (28) while the analytical curves are obtained from (31) with $i = 1$. As can be seen from the figure, NOMA with an INR level equal to −10 dB outperforms the other remaining scenarios, since it can ensure that the outage is achievable by all the users as controlling impacts of ICI.

Figure 6 demonstrates the outage performance for user 2 versus SNR with different INR levels. Similarly, the simulation curves can be obtained via (24) with the optimal β in

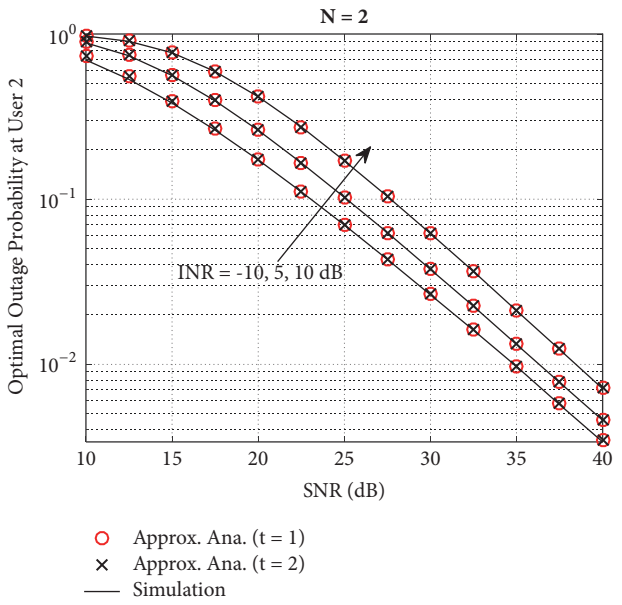

FIGURE 6: Optimal outage probability at user 2 vs. the average SNR.

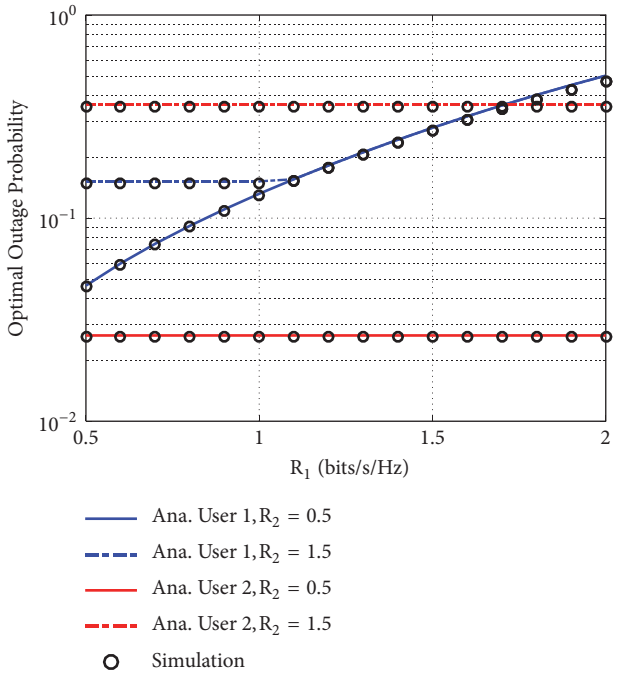

FIGURE 7: Optimal outage probability vs. user 1's target data rate.

(28) while the analytical curves are obtained from (31) with $i = 2$. One can observe that the proposed method achieves the lowest outage since it has the lowest impacts on the system among three scenarios. The figure also demonstrates the existence of the outage ceilings in the low SNR region (i.e., SNR less than 10 dB). This is due to the fact that the system probability is approaching an outage event and such outage is determined only by the SNR while other parameters do not affect outage. It is worth noting that increasing SNR can improve the outage; however, for the case INR $= -10$ dB,

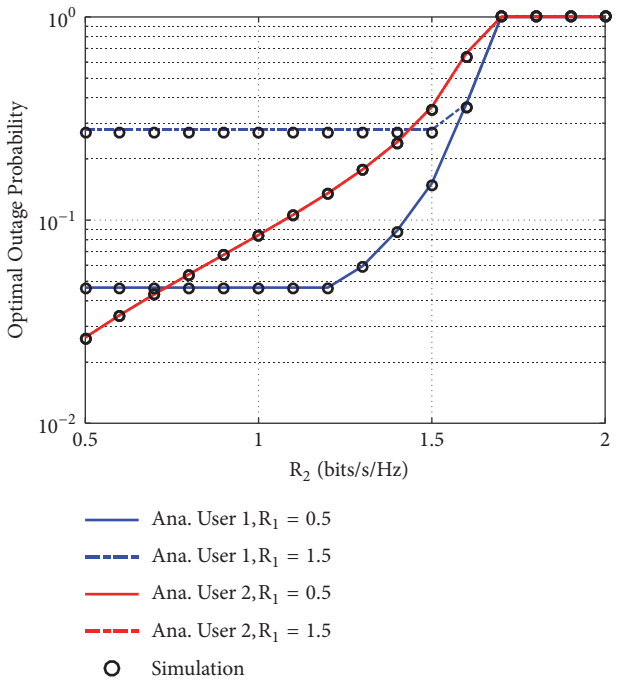

FIGURE 8: Optimal outage probability vs. user 2's target data rate.

the throughput is the lowest among three scenarios. This is because, in the latter case, the lower impact for information processing at user 2, and hence an outage, will be improved. Therefore, we see that it is important to select appropriate ICI when designing practical NOMA downlink transmission systems.

Figures 7 and 8 illustrate the optimal outage probability of both users versus the target rates, i.e., R_1 and R_2, in two different time blocks. The red and blue solid lines are both obtained from (31) when $i = 1$ (ensuring QoS at user 1) and $i = 2$ (ensuring QoS at user 2), respectively, while the simulation results for user 1 and user 2 are obtained by substituting $\beta = (1 + \sqrt{\eta|h_{ru_1}|^2})^{-1}$ into (22) and $\beta = (1 + \sqrt{\eta|h_{ru_2}|^2})^{-1}$ into (24), respectively. It is worth noting that, in the same signal block, the relay only satisfies QoS criteria for one user only; however we intend to compare the optimal outage performance each user can achieve. Firstly, one can observe that the outage probabilities of user 2 and user 1 can increase as R_2 and R_1 increase, respectively. The reason is that increasing R_2 and R_1 can lead to the higher threshold of decoding and therefore can result in more outage. More specifically, the outage probability at user 2 increases as R_2 increases but it remains constant varying R_1 as depicted in Figure 8, where the solid line overlaps the dashed line. The reason is that the performance of this user only depends on the data rate of x_2 but not that of x_1. In addition, the outage probability at user 1 depends highly on T_1; thus if $T_1 = \tau_1/\alpha_1$ increasing R_2 will not affect the outage probability at this user resulting in a segment of straight blue lines in Figure 8 and a portion of the blue curves in Figure 7, where the solid curve

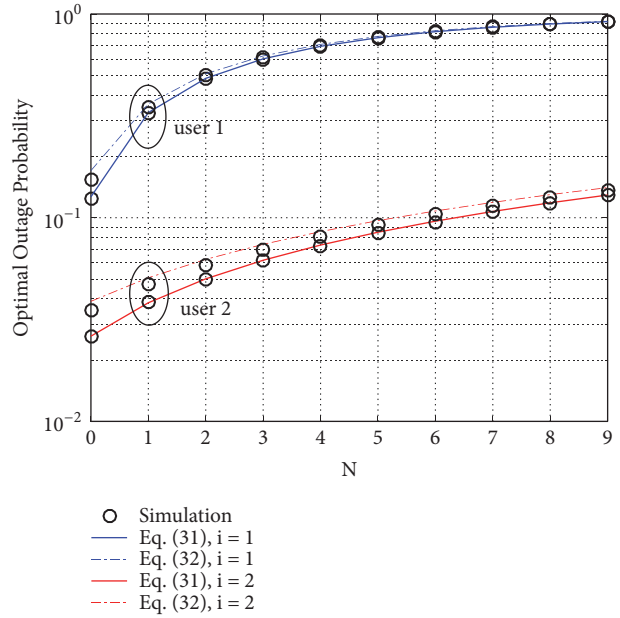

FIGURE 9: Optimal outage probability vs. number of external interferers.

overlaps the dashed curve. However, the system performance can be decreased in case of $T_1 = \tau_2/\alpha_2 - \tau_2\alpha_1$.

Figure 9 presents the optimal outage probability at both users as considering on increasing number of interferers. The solid curves are obtained through (31) representing the optimal outage probability of user i ($i = 1, 2$) whereas the dashed curves are achieved via (32) denoting the outage probability of user i when the relay focuses on optimizing the QoS of the other user, i.e., user $\bar{i}$. In such experiment, $I_{\psi_I}(\kappa)$ can be extracted from (21) as $m_1 = \ldots = m_N = 1$ and $\Omega_1 = \ldots = \Omega_N = 1$ (i.i.d. scenario). It is confirmed that if we try to optimize the outage probability for a user then another user cannot achieve maximum performance. This situation is equivalent to the case of requirement for maximum QoS for the selected user (i.e., user 1) resulting in system performance of the remaining user (i.e., user 2) being dropped.

6. Conclusions

In this paper, the application of simultaneously wireless information and power transfer (SWIPT) in nonorthogonal multiple access (NOMA) under the influence of external interferers has been investigated. In particular, we derived the closed-form expression of outage probability in the SWIPT NOMA protocol. In order to provide a complete framework, we illustrate system performance through simulation results used to address the impacts of the target rates of the near and far users and the number of interference sources and turn in evaluating the outage performance of the proposed protocol. In terms of outage probability, new analytical results have been derived to conclude the system efficiency. Such numerical results have been demonstrated to corroborate our analysis. We conclude that, by carefully choosing the parameters of the network regarding external interferers, acceptable system performance can be ensured by applying the SWIPT NOMA protocol in practical networks.

Appendix

A. Proof of Theorem 4

The characteristic function of Y is given by

$$\begin{aligned}\Phi_Y(j\omega) &= \mathbb{E}\left[e^{j\omega Y}\right] = \mathbb{E}\left[e^{j\omega\sum_{n=1}^{N} X_n}\right] \\ &= \prod_{n=1}^{N}\int_0^{\infty} e^{j\omega\varphi} f_{X_n}(\varphi)\, d\varphi \\ &= \prod_{n=1}^{N}\frac{1}{(1 - j\omega\mu_n)^{m_n}},\end{aligned} \tag{A.1}$$

where $j = \sqrt{-1}$ and $\gamma_n = P_n|h_n|^2$. The third equality is obtained by using the PDF of γ_n which is given by

$$f_{\gamma_n}(\varphi_n) = \frac{1}{\Gamma(m_n)\,\mu_n^{m_n}}\varphi_n^{m_n-1}\exp\left(-\frac{\varphi_n}{\mu_n}\right). \tag{A.2}$$

In addition, $\Phi_Y(j\omega)$ can be rewritten in terms of P distinct elements of μ_n in descending order as

$$\Phi_Y(j\omega) = \prod_{p=1}^{P}\frac{1}{\left(1 - j\omega\mu_{\langle p\rangle}\right)^{m_{\langle p\rangle}}}. \tag{A.3}$$

The PDF of Y is obtained through the characteristic function in (A.3) as

$$\begin{aligned} f_Y^{[2]}(\gamma) &= \frac{1}{2\pi}\int_{-\infty}^{\infty} e^{-j\omega x}\Phi_Y(j\omega)\, d\omega \\ &= \frac{1}{2\pi}\prod_{p=1}^{P}\int_{-\infty}^{\infty}\frac{e^{j\omega\gamma}}{\left(1 + j\omega\mu_{\langle p\rangle}\right)^{m_{\langle p\rangle}}} d\omega \\ &\overset{(a)}{=\!=} \frac{1}{2\pi}\sum_{p=1}^{P}\sum_{q=1}^{m_{\langle p\rangle}} R_{p,q}(\mathcal{S})\int_{-\infty}^{\infty}\frac{e^{j\omega\gamma}}{\left(1 + j\omega\mu_{\langle p\rangle}\right)^{q}} d\omega \\ &\overset{(b)}{=\!=} \sum_{p=1}^{P}\sum_{q=1}^{m_{\langle p\rangle}}\frac{R_{p,q}(\mathcal{S})}{(q-1)!\,\mu_{\langle p\rangle}^{q}}\gamma^{q-1}\exp\left(-\frac{\gamma}{\mu_{\langle p\rangle}}\right), \end{aligned} \tag{A.4}$$

where (a) is obtained by using partial fraction decomposition of (A.3) [26] and (b) is achieved with the help of [26, Eq. 3.382.6]. In addition, when $P = 1$, i.e., $\mu_1 = \mu_2 = \ldots \mu_N$, $R_{p,q}(\mathcal{S})$ becomes

$$R_{1,q}(\mathcal{S}) = \begin{cases} 0, & q = 1, 2, \ldots, m-1 \\ 1, & q = m. \end{cases} \tag{A.5}$$

The proof leads to the same result as in Theorem 4.

B.

Define $\delta_p(\upsilon) \triangleq (1+\upsilon\mu_{\langle p\rangle})^{-m_{\langle p\rangle}}$; the n-th derivative of $\delta_p(\upsilon)$ is given by

$$\delta_p^{(n)}(\upsilon) = (-1)^n \frac{\left(m_{\langle p\rangle}+n-1\right)!}{\left(m_{\langle p\rangle}-1\right)!} \frac{\mu_{\langle p\rangle}^n}{\left(1+\upsilon\mu_{\langle p\rangle}\right)^{m_{\langle p\rangle}+n}}. \quad \text{(B.1)}$$

Proof. In case of $n = 0$, it is obvious that $\delta_p^{(0)}(\upsilon) = \delta_p(\upsilon)$, which satisfies (B.1). In another case, assuming that $n = k$ holds, it can be proved that $n = k+1$ holds for $k \in \mathbb{N}$. It is noted that the $(k+1)$-*th* derivative of $\delta_p(\upsilon)$ is obtained as

$$\begin{aligned}\delta_p^{(k+1)}(\upsilon) &= \left[\delta_p^{(k)}(\upsilon)\right]^{(1)} \\ &= (-1)^{k+1} \frac{\left(m_{\langle p\rangle}-1+k+1\right)!}{\left(m_{\langle p\rangle}-1\right)!} \frac{\mu_{\langle p\rangle}^{k+1}}{\left(1+\upsilon\mu_{\langle p\rangle}\right)^{m_{\langle p\rangle}+k+1}}.\end{aligned} \quad \text{(B.2)}$$

Therefore, using the induction hypothesis, (B.1) holds for all $k \in \mathbb{N}$.

Define $\mathscr{L}_p(\upsilon) \triangleq \prod_{k=1,k\neq p}^{P} \delta_k(\upsilon)$; then according to Leibniz's rule [26], the *n-th* derivative of $\mathscr{L}(\upsilon)$ is given as

$$\begin{aligned}\mathscr{L}_p^{(n)}(\upsilon) &= \sum_{\{n_k\}_{k=1,k\neq p}^{P}}^{n} \prod_{k=1,k\neq p}^{P} \binom{n_{k-1}}{n_k} \delta_k^{(n_k)}(\upsilon) \\ &= \sum_{n_1=0}^{n} \binom{n}{n_1} \cdots \sum_{\substack{n_k=0 \\ k\neq p}}^{n_{k-1}} \binom{n_{k-1}}{n_k} \\ &\quad \cdots \sum_{n_P=0}^{n_{P-1}} \binom{n_{P-1}}{n_P} \prod_{\substack{k=1 \\ k\neq p}}^{P} \delta_k^{(n_k)}(\upsilon).\end{aligned} \quad \text{(B.3)}$$

Substituting (B.3) into (18) $R_{p,q}(\mathcal{S})$ is rewritten for $P \geq 1$ as

$$R_{p,q}(\mathcal{S}) = \frac{\mathscr{L}_p^{(m_{\langle p\rangle}-q)}\left(-1/\mu_{\langle p\rangle}\right)}{\left(m_{\langle p\rangle}-q\right)!\mu_{\langle p\rangle}^{m_{\langle p\rangle}-q}}. \quad \text{(B.4)}$$

□

C. Proof of (22)

Substituting (9) and (10) into (22), after some algebraic steps, we can obtain

$$\begin{aligned}\overline{\mathcal{O}}_1 &= \Pr\{\gamma_{1\longrightarrow 2} > \tau_2, \gamma_1 > \tau_1\} = \Pr\left\{\psi_{sr}\right. \\ &> \frac{\tau_2}{\alpha_2 - \tau_2\alpha_1}\left(\psi_I + \frac{1}{\psi_{ru_1}} + \frac{1}{1-\beta}\right), \psi_{sr} \quad \text{(C.1)} \\ &\left. > \frac{\tau_1}{\alpha_1}\left(\psi_I + \frac{1}{\psi_{ru_1}} + \frac{1}{1-\beta}\right)\right\} \\ &= \Pr\left\{\psi_{sr} > \mathrm{T}_1\left(\psi_I + \frac{1}{\psi_{ru_1}} + \frac{1}{1-\beta}\right)\right\}. \quad \text{(C.2)}\end{aligned}$$

The CDF of ψ_{sr} and the PDF of the ordered ψ_{ru_1} [28] are given by

$$F_{\psi_{sr}}(\gamma) = 1 - \exp\left(-\frac{\gamma}{\mu_{SR}}\right), \quad (\gamma \geq 0) \quad \text{(C.3)}$$

$$f_{\psi_{ru_1}}(\gamma) = \sum_{k=1}^{3} \frac{(-1)^{k-1}}{\mu_k} \exp\left(-\frac{\gamma}{\mu_k}\right), \quad (\gamma \geq 0). \quad \text{(C.4)}$$

Substituting (C.2) and (C.3) into (C.1) we obtain

$$\begin{aligned}&\overline{\mathcal{O}}_1 \\ &= \exp\left(-\frac{\mathrm{T}_1}{\mu_{sr}}\frac{1}{1-\beta}\right)\int_0^\infty \exp\left(-\frac{\mathrm{T}_1}{\mu_{sr}}\gamma\right) f_{\psi_I}(\gamma)\, d\gamma \quad \text{(C.5)} \\ &\quad \times \sum_{k=1}^{3} \frac{(-1)^{k-1}}{\mu_k} \int_0^\infty \exp\left(-\frac{\mathrm{T}_1}{\mu_{sr}}\frac{1}{\gamma} - \frac{\gamma}{\mu_k}\right) d\gamma,\end{aligned}$$

where the first integral is obtained by adopting Proposition 2 and the second integral is obtained with the help of [26, Eq. 3.471.9]. Therefore, (C.5) immediately follows (23).

D. Proof of (31)

First, let us rewrite the PDF of the ordered channels, $|h_i|^2$ $(i = 1, 2)$, as

$$f_{|h_i|^2}(x) = \sum_{k=i}^{4-i} \frac{(-1)^{k+\bar{i}-1}}{\Omega_k} \exp\left(-\frac{x}{\Omega_k}\right). \quad \text{(D.1)}$$

From (C.2) and (26), we can see the similarities of the two equations, and, therefore, it is possible to achieve a unified equation to determine the coverage probability at user u_i which is given by

$$\overline{\mathcal{O}}_i = \Pr\left\{\psi_{sr} > \mathrm{T}_i\left(\psi_I + \frac{1}{\psi_{ru_i}} + \frac{1}{1-\beta}\right)\right\}. \quad \text{(D.2)}$$

Substituting (30) into (D.2), using similar steps in Appendix A, the above equality is rewritten as follows:

$$\overline{\mathcal{O}}_i = 1 - \mathrm{I}_{\psi_I}\left(\frac{\mathrm{T}_i}{\mu_{sr}}\right)\exp\left(-\frac{\mathrm{T}_i}{\mu_{sr}}\right)\times\sum_{k=i}^{4-i}\frac{(-1)^{k+\bar{i}-1}}{\Omega_k} \cdot\int_0^{\infty}\exp\left(-\frac{\mathrm{T}_i}{\mu_{sr}\eta}\frac{2}{\sqrt{y}}-\frac{\mathrm{T}_i}{\mu_{sr}\eta}\frac{1}{y}-\frac{1}{\Omega_k}y\right)dy. \tag{D.3}$$

The above equation cannot be expressed in closed form; however it is noticed that when $x \longrightarrow 0$ the exponential function is approximated as

$$\exp(-x) \simeq 1 - x. \tag{D.4}$$

Applying (D.4) into (D.3), $\overline{\mathcal{O}}_i$ is approximated as

$$\overline{\mathcal{O}}_i \simeq 1 - \mathrm{I}_{\psi_I}\left(\frac{\mathrm{T}_i}{\mu_{sr}}\right)\exp\left(-\frac{\mathrm{T}_i}{\mu_{sr}}\right)\sum_{k=i}^{4-i}\frac{(-1)^{k+\bar{i}-1}}{\Omega_k} \times\left[\int_0^{\infty}\exp\left(-\frac{\mathrm{T}_i}{\mu_{sr}\eta}\frac{1}{y}-\frac{1}{\Omega_k}y\right)dy - 2\frac{\mathrm{T}_i}{\mu_{sr}\eta}\int_0^{\infty}\frac{1}{\sqrt{y}}\exp\left(-\frac{\mathrm{T}_i}{\mu_{sr}\eta}\frac{1}{y}-\frac{1}{\Omega_k}y\right)dy\right]. \tag{D.5}$$

One can utilize [26, Eq. 3.471.9] and [26, Eq. 3.471.15] to solve the first and second integral, respectively. Therefore, after some algebraic manipulations we then achieve (31).

E. Proof of (32)

From (D.2) and (30) the coverage probability of the other user is given by

$$\overline{\mathcal{O}}_{\bar{i}} = \Pr\left\{\psi_{sr} > \mathrm{T}_{\bar{i}}\left(\psi_I + \frac{1+\sqrt{\eta\left|h_{ru_i}\right|^2}}{\eta\left|h_{ru_{\bar{i}}}\right|^2} + \frac{1+\sqrt{\eta\left|h_{ru_i}\right|^2}}{\sqrt{\eta\left|h_{ru_i}\right|^2}}\right)\right\}. \tag{E.1}$$

Substituting (D.1) and adopting Theorem 6 into (E.1), we then have

$$\overline{\mathcal{O}}_{\bar{i}} = \mathrm{I}_{\psi_I}\left(\frac{\mathrm{T}_{\bar{i}}}{\mu_{sr}}\right)\exp\left(-\frac{\mathrm{T}_{\bar{i}}}{\mu_{sr}}\right)\times\int_0^{\infty}\left\{\exp\left(-\frac{\mathrm{T}_{\bar{i}}}{\mu_{sr}}\frac{1}{\eta y}\right) \cdot f_{|h_{ru_{\bar{i}}}|^2}(y)\times\int_0^{\infty}\exp\left[-\frac{\mathrm{T}_{\bar{i}}}{\mu_{sr}\sqrt{\eta}}\left(\frac{\sqrt{x}}{y}+\frac{1}{\sqrt{x}}\right)\right] \cdot f_{|h_{ru_i}|^2}(x)\,dx\right\}dy. \tag{E.2}$$

Adopting (D.1) and (D.4) into (E.2), $\overline{\mathcal{O}}_{\bar{i}}$ is obtained approximately as

$$\overline{\mathcal{O}}_{\bar{i}} \simeq \mathrm{I}_{\psi_I}\left(\frac{\mathrm{T}_{\bar{i}}}{\mu_{sr}}\right)\exp\left(-\frac{\mathrm{T}_{\bar{i}}}{\mu_{sr}}\right)\sum_{k_{\bar{i}}=\bar{i}}^{4-\bar{i}}\sum_{k_i=i}^{4-i}\left\{\frac{(-1)^{k_{\bar{i}}+i-1}}{\Omega_{k_{\bar{i}}}}\times\frac{(-1)^{k_i+\bar{i}-1}}{\Omega_{k_i}} \cdot\int_0^{\infty}\exp\left(-\frac{\mathrm{T}_{\bar{i}}}{\mu_{sr}}\frac{1}{\eta y}\right)\exp\left(-\frac{y}{\Omega_{k_{\bar{i}}}}\right)\times\left[\Omega_{k_i}-\int_0^{\infty}\frac{\mathrm{T}_{\bar{i}}}{\mu_{sr}\sqrt{\eta}}\frac{1}{\sqrt{x}}\exp\left(-\frac{x}{\Omega_{k_i}}\right)dx-\int_0^{\infty}\frac{\mathrm{T}_{\bar{i}}}{\mu_{sr}\sqrt{\eta}}\frac{\sqrt{x}}{y}\exp\left(-\frac{x}{\Omega_{k_i}}\right)dx\right]dy\right\}. \tag{E.3}$$

By applying [26, Eq. 3.371] to solve the second and third integral, we then achieve

$$\overline{\mathcal{O}}_{\bar{i}} \simeq \mathrm{I}_{\psi_I}\left(\frac{\mathrm{T}_{\bar{i}}}{\mu_{sr}}\right)\exp\left(-\frac{\mathrm{T}_{\bar{i}}}{\mu_{sr}}\right) \cdot\sum_{k_{\bar{i}}=\bar{i}}^{4-\bar{i}}\sum_{k_i=i}^{4-i}\left\{\frac{(-1)^{k_{\bar{i}}+i-1}}{\Omega_{k_{\bar{i}}}}\times(-1)^{k_i+\bar{i}-1}\int_0^{\infty}\left[\exp\left(-\frac{\mathrm{T}_{\bar{i}}}{\mu_{sr}\eta}\frac{1}{y}-\frac{y}{\Omega_{k_{\bar{i}}}}\right)\times\left(1-\frac{\mathrm{T}_{\bar{i}}}{\mu_{sr}}\sqrt{\frac{\pi}{\eta\Omega_{k_i}}}-\frac{1}{2}\frac{\mathrm{T}_{\bar{i}}}{\mu_{sr}}\sqrt{\frac{\pi\Omega_{k_i}}{\eta}}\frac{1}{y}\right)dy\right]\right\}, \tag{E.4}$$

where the integral part in (E.4) can be evaluated in closed form by adopting [[26], Eq. 3.471.9]. Hence, after some manipulations, we then get (32).

Data Availability

The data used to support the findings of this study are available from the corresponding author upon request.

Conflicts of Interest

The authors declare that there are no conflicts of interest regarding the publication of this paper.

References

[1] Y. Saito, A. Benjebbour, Y. Kishiyama, and T. Nakamura, "System-level performance evaluation of downlink non-orthogonal multiple access (NOMA)," in *Proceedings of the 2013 IEEE 24th Annual International Symposium on Personal, Indoor, and Mobile Radio Communications, PIMRC*, pp. 611–615, September 2013.

[2] Z. Ding, Z. Yang, P. Fan, and H. V. Poor, "On the performance of non-orthogonal multiple access in 5G systems with randomly deployed users," *IEEE Signal Processing Letters*, vol. 21, no. 12, pp. 1501–1505, 2014.

[3] J. Choi, "Non-orthogonal multiple access in downlink coordinated two-point systems," *IEEE Communications Letters*, vol. 18, no. 2, pp. 313–316, 2014.

[4] Z. Ding, M. Peng, and H. V. Poor, "Cooperative Non-Orthogonal Multiple Access in 5G Systems," *IEEE Communications Letters*, vol. 19, no. 8, pp. 1462–1465, 2015.

[5] Q. Sun, S. Han, I. Chin-Lin, and Z. Pan, "On the Ergodic Capacity of MIMO NOMA Systems," *IEEE Wireless Communications Letters*, vol. 4, no. 4, pp. 405–408, 2015.

[6] J.-B. Kim and I.-H. Lee, "Capacity Analysis of Cooperative Relaying Systems Using Non-Orthogonal Multiple Access," *IEEE Communications Letters*, vol. 19, no. 11, pp. 1949–1952, 2015.

[7] Z. Qin, Y. Liu, Z. Ding, Y. Gao, and M. Elkashlan, "Physical layer security for 5G non-orthogonal multiple access in large-scale networks," in *Proceedings of the ICC 2016 - 2016 IEEE International Conference on Communications*, pp. 1–6, Kuala Lumpur, Malaysia, May 2016.

[8] Y. Liu, Z. Qin, M. Elkashlan, Y. Gao, and L. Hanzo, "Enhancing the Physical Layer Security of Non-Orthogonal Multiple Access in Large-Scale Networks," *IEEE Transactions on Wireless Communications*, vol. 16, no. 3, pp. 1656–1672, 2017.

[9] B. He, A. Liu, N. Yang, and V. K. N. Lau, "On the Design of Secure Non-Orthogonal Multiple Access Systems," *IEEE Journal on Selected Areas in Communications*, vol. 35, no. 10, pp. 2196–2206, 2017.

[10] X.-X. Nguyen and D.-T. Do, "Maximum harvested energy policy in full-duplex relaying networks with SWIPT," *International Journal of Communication Systems*, vol. 30, no. 17, 2017.

[11] N. T. Luan and D.-T. Do, "A new look at AF two-way relaying networks: energy harvesting architecture and impact of co-channel interference," *Annals of Telecommunications-Annales des Télécommunications*, vol. 72, no. 11-12, pp. 669–678, 2017.

[12] D.-T. Do and C.-B. Le, "Application of NOMA in Wireless System with Wireless Power Transfer Scheme: Outage and Ergodic Capacity Performance Analysis," *Sensors*, vol. 18, no. 10, p. 3501, 2018.

[13] D.-T. Do, H.-S. Nguyen, M. Voznak, and T.-S. Nguyen, "Wireless powered relaying networks under imperfect channel state information: System performance and optimal policy for instantaneous rate," *Radioengineering*, vol. 26, no. 3, pp. 869–877, 2017.

[14] D.-T. Do, "Power switching protocol for two-way relaying network under hardware impairments," *Radioengineering*, vol. 24, no. 3, pp. 765–771, 2015.

[15] Y. Liu, Z. Ding, M. Elkashlan, and H. V. Poor, "Cooperative Non-orthogonal Multiple Access with Simultaneous Wireless Information and Power Transfer," *IEEE Journal on Selected Areas in Communications*, vol. 34, no. 4, pp. 938–953, 2016.

[16] N. T. Do, D. B. Da Costa, T. Q. Duong, and B. An, "A BNBF User Selection Scheme for NOMA-Based Cooperative Relaying Systems with SWIPT," *IEEE Communications Letters*, vol. 21, no. 3, pp. 664–667, 2017.

[17] D.-T. Do and H.-S. Nguyen, "A tractable approach to analyzing the energy-aware two-way relaying networks in the presence of co-channel interference," *EURASIP Journal on Wireless Communications and Networking*, vol. 2016, no. 1, 2016.

[18] S. S. Ikki and S. Aissa, "Performance analysis of two-way amplify-and-forward relaying in the presence of co-channel interferences," *IEEE Transactions on Communications*, vol. 60, no. 4, pp. 933–939, 2012.

[19] I. Trigui, S. Affes, and A. Stéphenne, "Ergodic capacity of two-hop multiple antenna AF systems with co-channel interference," *IEEE Wireless Communications Letters*, vol. 4, no. 1, pp. 26–29, 2015.

[20] H. Alves, C. de Lima, P. Nardelli, R. Souza, and M. Latva-aho, "On the Average Spectral Efficiency of Interference-Limited Full-Duplex Networks," in *Proceedings of the 9th International Conference on Cognitive Radio Oriented Wireless Networks*, 554, 550 pages, Oulu, Finland, June 2014.

[21] H. Alves, R. D. Souza, D. B. da Costa, and M. Latva-aho, "Full-Duplex Relaying Systems Subject to Co-Channel Interference and Noise in Nakagami-m Fading," in *Proceedings of the 2015 IEEE 81st Vehicular Technology Conference (VTC Spring)*, pp. 1–5, Glasgow, United Kingdom, May 2015.

[22] G. Sharma, P. K. Sharma, and P. Garg, "Performance analysis of full duplex relaying in multicell environment," in *Proceedings of the 2014 International Conference on Advances in Computing, Communications and Informatics (ICACCI)*, pp. 2501–2505, Delhi, India, September 2014.

[23] D. Benevides da Costa, . Haiyang Ding, and . Jianhua Ge, "Interference-Limited Relaying Transmissions in Dual-Hop Cooperative Networks over Nakagami-m Fading," *IEEE Communications Letters*, vol. 15, no. 5, pp. 503–505, 2011.

[24] D. B. da Costa and M. D. Yacoub, "Outage performance of two hop AF relaying systems with co-channel interferers over Nakagami-m fading," *IEEE Communications Letters*, vol. 15, no. 9, pp. 980–982, 2011.

[25] D. B. Da Costa, H. Ding, M. D. Yacoub, and J. Ge, "Two-way relaying in interference-limited AF cooperative networks over nakagami-m fading," *IEEE Transactions on Vehicular Technology*, vol. 61, no. 8, pp. 3766–3771, 2012.

[26] A. Jeffrey and D. Zwillinger, *Table of integrals, series, and products*, Academic press, 2007.

[27] H. A. David and H. N. Nagaraja, *Order Statistics*, John Wiley, New York, NY, USA, 3rd edition, 2003.

[28] Z. Yang, Z. Ding, P. Fan, and N. Al-Dhahir, "The Impact of Power Allocation on Cooperative Non-orthogonal Multiple Access Networks with SWIPT," *IEEE Transactions on Wireless Communications*, vol. 16, no. 7, pp. 4332–4343, 2017.